Droplet Surface Immunoassay by Relocation (D-SIRe) for High-Throughput Analysis of Cytosolic Proteins at the Single-Cell Level

Robin Dufossez, Sylvain Ursuegui, Stéphanie Baudrey, Ketty Pernod, Safae Mouftakhir, Mustapha Oulad-Abdelghani, Michel Mosser, Guilhem Chaubet, Michaël Ryckelynck, Alain Wagner

Droplet Surface ImmunoAssay by Relocation (D-SIRe) for high throughput analysis of cytosolic proteins at the single cell level

Robin Dufossez[1], Sylvain Ursuegui[1], Stephanie Baudrey[2], Ketty Pernod[1], Safae Mouftakhir[1], Mustapha Oulad-Abdelghani[3], Michel Mosser[1], Guilhem Chaubet[1], Michael Ryckelynck[2], Alain Wagner[1*]

[1]Bio-Functional Chemistry (UMR 7199), Institut du Médicament de Strasbourg, University of Strasbourg, 74 Route du Rhin, 67400 Illkirch-Graffenstaden, France (alwag@unistra.fr)

[2]Université de Strasbourg, CNRS, Architecture et Réactivité de l'ARN, UPR 9002, 67000 Strasbourg, France

[3]Institut de Génétique et de Biologie Moléculaire et Cellulaire (IGBMC), INSERM U 1258, CNRS UMR 7104, University of Strasbourg, 67404 Illkirch, France.

ABSTRACT: Enzyme Linked Immunosorbent Assay (ELISA) is a central analytic method in biological science for the detection of proteins. Introduction of droplet-based microfluidics allowed the development of miniaturized, less consuming and more sensitive ELISA assays, by co-encapsulating the biological sample and antibody-functionalized particles. We report herein, an alternative in-droplet immunoassay format, which avoids the use of particles. It exploits the oil/aqueous phase interface as a protein capture and detection surface. This is achieved by using tailored perfluorinated surfactant bearing azide functionalized PEG-based polar head groups which spontaneously react, when meeting at the droplet formation site, with strained alkyne functionalized antibodies solubilized in the water phase. The resulting Antibody-functionalized inner surface is then usable to capture a target protein. This surface capture process lead to concomitant relocation at the surface of a labelled detection antibody and in turn to a drastic change of the shape of the fluorescence signal from a convex shape (not captured) to a characteristic concave shape (captured). This novel Droplet Surface Immunoassay by fluorescence Relocation (D-SIRe) proved to be fast and sensitive at 2.3 attomoles of analyte per droplet. It was further demonstrated to allow detection of cytosolic proteins at the single bacteria level.

Introduction

Technologies for detecting and identifying proteins are ubiquitous in biological research, enabling to decipher complex secretion-induced mechanisms, to set-up screening methods in drug discovery or to establish diagnostic protocols.[1] The prevalent approaches to detect proteins rely on mass spectrometry[2] and immunoassays.[3,4] Among them, the most commonly used is the Enzyme-Linked Immunosorbent Assay (ELISA)[5] and especially its ELISA sandwich version, in which two antibodies bind to the protein of interest (the antigen, Ag) at two distinct epitopes. In this approach, one of the antibodies is immobilized in excess on a surface (the capture Ab), while the second (detection Ab) is used to detect and quantify the protein already bound to the capture Ab.[5] Conventional ELISA sandwich assays are usually performed by coating the surface of microwells plates with the capture Ab while the detection Ab is added in solution after the protein capture step. Even when tiny microliter-well are used this ELISA format suffers from certain limitations in terms of throughput, automation, volume of reagent, cost of consumables and, often, high limit of detection (LOD).[6,7]

In order to improve the LOD, the capture Ab can be coated on microspheres or microbeads which are added in the well. It provides a much lower surface/volume ratio (thus more concentrated signal) as compared with coated plastic surface (**Figure 1A-B**).[3,6,7] This moreover allows to reduce the amount of Ab used and therefore the cost. This strategy was further adapted to droplet-based microfluidics (**Figure 1C**), resulting in a drastic miniaturization of the process, improving the sensitivity of the assays, reducing sample consumption, and increasing the analysis speed.[8] Indeed, in this format, each analysis is performed in sub-nanoliter volumes at ultrahigh-throughput rates of thousands events per second.[9] Such approach, for instance, enabled Cohen *et al.* to develop an in-droplet ELISA sensitive at attomole concentration.[10] Related bead-in-droplet strategy enabled the analysis and sorting of antibody-secreting[9] hybridomas or B cells.[11,12] The use of beads comes however with some limitations. First, depending on the size of the beads and of the material they are made of, it may be difficult to control precisely the number of beads per droplet.[8,13] Secondly, and more problematically, the detection of a signal emitted by particles (beads or even cells) that are free to move within droplets can cause inter-droplet consistency issues. As conventional microfluidic analysis workstations use laser beams (or line) focussed within the droplet, the bead's signal can strongly vary depending on the distance between the particle and the maximum excitation volume. Therefore, unless complex optical set-ups are used (e.g., a light sheet), distributed measurements are often obtained even for highly similar objects.[14] To address these two important limitations, while conserving the ultrahigh-throughput capacity, we investigated the possibility of directly using the extended water-oil droplet interface[15] as a surface to graft/coat the capture antibody (**Figure 1D**). In this scheme, bead's distribution in droplets would not be a concern anymore, and the targeted protein could be directly detected by measuring the magnitude of signal relocation at the homogeneously coated droplet inner surface.

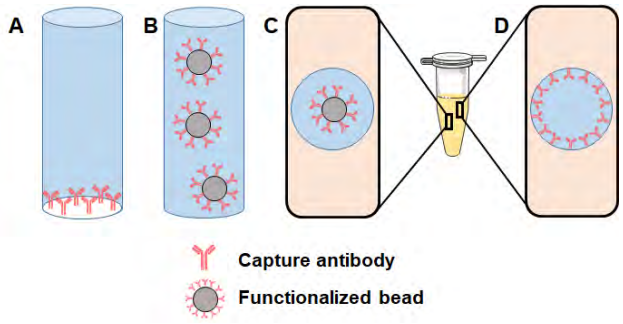

Figure 1. Schematic illustration of different ELISA sandwich formats. Only the immobilized antibody (capture antibody) is represented in the figure. **A)** Microplate well coated with capture antibodies. **B)** Microplate well with Ab-coated microbeads. **C)** Droplet based microfluidics immunoassay, with the encapsulation of functionalized microbeads to capture the antigen. **D)** This work: droplet-based microfluidics immunoassay, using the inner water-oil interface as a reactive surface to covalently attach the capture antibody.

In droplet microfluidics, using a surfactant is required to obtain mono-disperse, stable and biocompatible droplets.[16,17] Hence surfactant optimisation was conducted in order to reduce as much as possible droplet leaking and droplet coalescence. In 2009 Kreutz J. E. *et al.* reported a surfactant with nitrilotriacetate nickel complex and used it to induce crystallisation of HisTag proteins at the droplets' inner surface.[18] Inspired by this work we first designed a versatile mono-azide fluorosurfactant able to capture small molecular probes *via* a Strain Promoted Azide Alkyne Cycloaddition (SPAAC).[19] In the same vein, Chowdhury *et al.* recently designed a fluorosurfactant bearing azide moieties able to capture a protein complex formed with dibenzocyclooctyne (DBCO)-biotin and streptavidin.[20]

Exploiting further the possibility to decorate the inner surface of the droplets with biomolecules *via* biorthogonal click chemistry, we report herein the design and synthesis of molecular tools and detection method enabling intra-droplet analysis of protein at the single cell level.

Results and discussion

Preparation of conjugated antibodies

To be able to both graft the Ab at droplet surface and track their intra-droplet location, antibodies were bi-functionalized by reaction with a mixture of an activated ester of (BCN)-PEG$_4$ linker and an activated ester of cyanine fluorophore (disulfo-Cy5 or disulfo-Cy3). (**Figure 2**) While the strained alkyne is needed for the SPAAC to proceed, the fluorophore allows to assess the efficiency of this grafting process by visualizing Ab localization in the droplet.

Such lysine-type bioconjugation results in a stochastic distribution of the BCN to antibodies ratio. Hence the average number of BCN *per* antibody will be indicated by its Degree Of Conjugation (DOC). Different sample of functionalized Trastuzumab were produced by performing the bioconjugation with increasing amount of activated ester while keeping the ratio fluorescent probe/Ab constant. This afforded samples of conjugated Ab with average number of BCN/Ab ranging from 0 to 5.

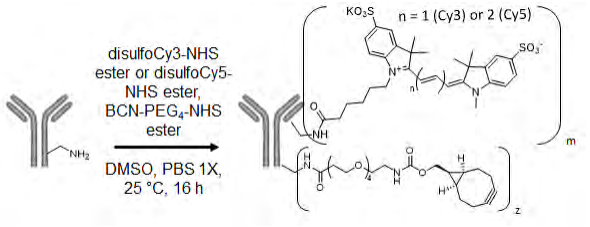

Figure 2. Antibody functionalization via lysine conjugation. The activated ester reagents react with the amine groups on the lateral chain of lysine residues to form an amide bond via a stochastic process. m is kept constant at 1 while z varies from 0 to 5.

These batches will allow to investigate the effect of the number of BCN per antibody on the completion of the grafting process (see Supporting Information for experimental details).

Design and synthesis of multivalent fluorosurfactants

Building on our previous work,[19] functionalized fluorosurfactants were designed with hydrophilic headgroups bearing various number of terminal azide functions (**Figure 3**).[19,21] Commercially available perfluoropolyether (PFPE) (Krytox 157FSH, Dupont) was used as the fluorophilic tail for all surfactants as it is widely described to provide efficient stabilization and monodisperse emulsions.[16,19,22,23] In order to avoid unspecific protein interaction and preserve biocompatibility,[24] Krytox is usually associated with a non-ionic hydrophilic head, such as polyethylene glycol (PEG).[16,17]

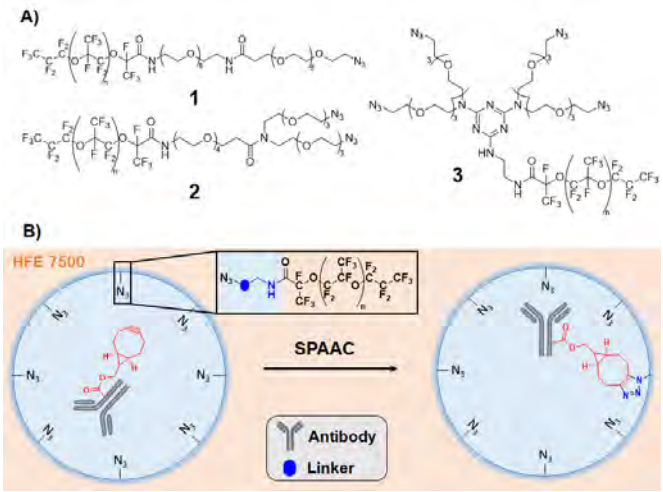

Figure 3. A) Structures of the functionalized fluorosurfactants **1**, **2** and **3. B)** Schematic illustration of the *in-droplet* Antibody grafting step: SPAAC reaction at the inner surface of the droplets with a strained alkyne conjugated biomolecule. The use of a functionalized surfactant allows to present a terminal azide moiety at the inner droplet surface. In the presence of a strained alkyne conjugated antibody, a SPAAC proceeds, leading to the relocalization of the antibody at the inner surface of the droplets.

We have previously published a mono-azide fluorosurfactant (**Figure 3A, (1)**), made of an azide-modified polyethylene glycol (PEG) hydrophilic head and a Krytox fluorophilic tail.[19] This monoazide PEG-fluorosurfactant was synthetized with a purity of up to 85% according to NMR analysis and previously demonstrated its ability to produce stable monodisperse droplets upon SPAAC reaction with a PEG-linked BCN-fluorophore (sulfoCy5, sulfoCy3).[19] However, when testing it, this surfactant proved to be inefficient for grafting fluorescently labelled BCN-modified antibodies (**Figure 4** and **Figure S1**). Indeed,

none of the antibodies prepared at different DOC of BCN lead to a relocation of fluorescence at the droplet surface. To improve the grafting efficacy, we thus decided to increase the density of azide moieties potentially available at the inner surface of the droplets. Two new hydrophilic headgroups, bearing respectively two and four azide groups were hence synthesized.

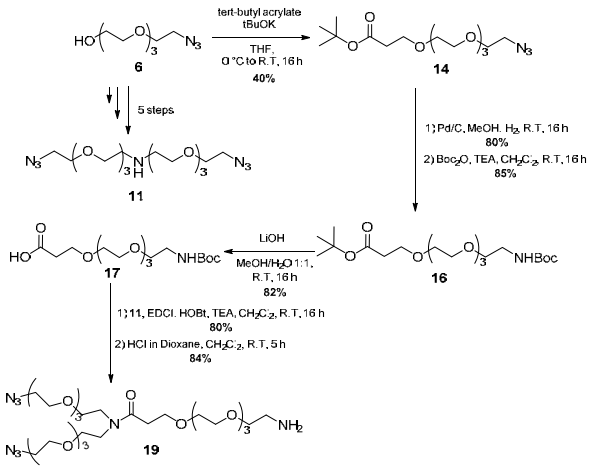

Scheme 1. Synthesis pathway of the hydrophilic head 19

Both new hydrophilic heads were synthetized using the building block diazide (**11**), obtained via our previously described reductive dimerization methodology.[21] The complete synthesis of the tetra-azide hydrophilic head used for surfactant (**3**) was previously described.[21] Briefly, the di-azide hydrophilic head was obtained *via* a six-step synthesis **(Scheme 1)**, starting from a Michael addition between **PEG$_3$N$_3$** (**6**) (obtained in two steps from commercial tetra ethylene glycol) and *tert*-butyl acrylate (see **Supporting Information 1.3**). The azide group of ester (**14**) was then reduced by catalytic hydrogenation to a primary amine that was next protected with a Boc group to obtain compound (**16**). The *tert*-butyl ester was then selectively hydrolysed under basic conditions to obtain the carboxylic acid (**17**). This linker was activated using EDC and HOBt and further reacted with the di-azide building block (**11**). After *N*-Boc deprotection, the resulting hydrophilic head (**19**) was isolated with an 84% yield. (**Figure S2**).

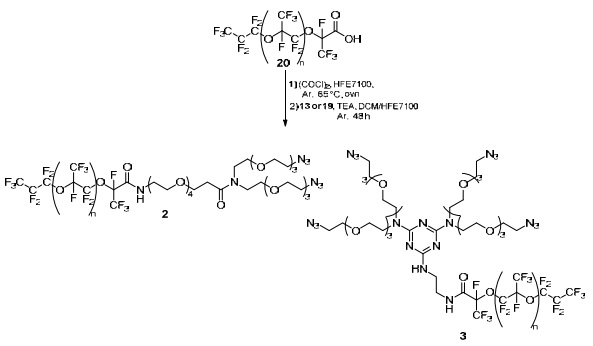

Scheme 2. Synthesis of fluorosurfactants 2 and 3

For the coupling step, Krytox 157FSH was activated with an excess of oxalyl chloride and reacted with the hydrophilic heads (**13**) or (**19**) in a mixture of CH_2Cl_2/Novec7100, to afford the surfactants (**2**) and (**3**) (**Scheme 2**). The efficiency of the coupling of Krytox 157FSH with the hydrophilic head was assessed by ^{19}F NMR, as reported by Holtze *et al.*[17,19] Several batches of surfactant (from 1 to 4 g) were synthetized, with a purity reaching up to 95% (characterizations by NMR spectroscopy are described in the **Supporting Information 1.4**).

SPAAC-mediated grafting of antibodies at the inner surface of the droplets

The capacity of the new multivalent surfactants (**2**) and (**3**) to elicit effective antibody grafting at droplet inner surface was evaluated using a fluorescently labelled version of the commercial IgG Trastuzumab as a model antibody (**Figure 4**). The bioconjugation reaction was optimized in order to determine the DOC (aDOC fig. 4A) needed to obtain a full relocation of the antibody at droplet's inner surface.

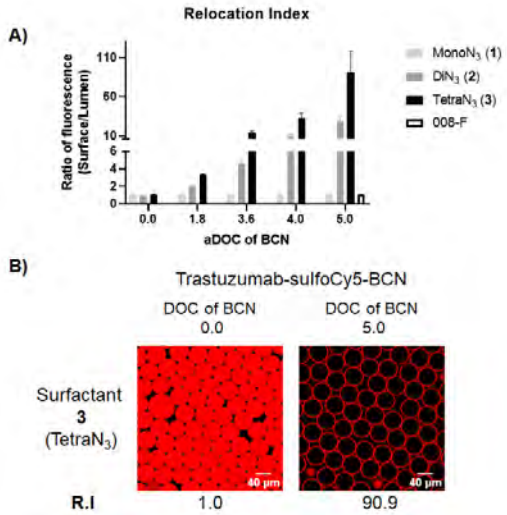

Figure 4. A) Comparison of the ratio of fluorescence (fluorescence in the content of the droplet vs fluorescence at the inner surface) obtained for droplets formed with fluorosurfactant **1**, **2** and **3** and Trastuzumab with increasing amount of BCN/Ab (aDOC). The ratio of fluorescence (Relocation Index, R.I.) (Droplet surface/Droplet content) is calculated by analysing confocal microscopy pictures of the different emulsions (*via* ImageJ). Since labelled antibodies relocalize to the inner surface during the grafting process, the higher the ratio, the higher the grafting efficiency. **B)** Confocal microscopy pictures presenting droplets without grafting or with a complete grafting and their R.I.

To evaluate the relocation of BCN-bearing Ab at the droplet's inner surface depending on the structure of the azide surfactant, emulsions of 45 pL droplets containing a 400 nM solution of fluorescently labelled Trastuzumab with different DOCs of BCN were produced. As controls, the same experiment was performed using non-functionalized surfactant 008-F (RAN Biotechnologies) or non-BCN-antibodies (DOC: 0). Upon collection, the droplets were incubated 1 h at room temperature and then analysed by confocal microscopy to the fluorescence distribution in the droplets (**Figure S1**). The grafting efficiency obtained with each surfactant was evaluated by computing the relocation index (R.I.) of the antibody in each condition. Briefly, the R.I. normalizes the fluorescence at droplet surface by the one found in its lumen (droplet content) (see **Supporting Information 2.4 for calculation detail**). Therefore, the more efficient the grafting, the higher the R.I. An R.I. above 20

means that above 95% of the antibodies are relocated at the inner surface of the droplets. As expected, in all tested conditions (DOC of BCN from 1.8 to 5.0), increasing the density of azide groups allowed to drastically improve antibody grafting as compared with the monoazide fluorosurfactant **1**. Indeed, having two azides per surfactant (diazide fluorosurfactant **2**) allowed grafting to be distinguishable at a DOC of 1.8 and to reach apparent completion at a DOC of 5 (**Figure 4** and **Figure S1**). Excitingly, increasing azide density to 4 azides per surfactant molecule (tetraazide fluorosurfactant **3**) increased antibody grafting even further, with a R.I. ~ three times higher from a DOC of BCN of 3.6 to 5.0, and reaching a R.I. of ~32 (close to R.I. of ~ 29 obtained with diazide fluorosurfactant **2** at a DOC of BCN of 5) at a DOC of BCN of only 4.0 (**Figure 4** and **Figure S1**). We confirmed that this complete grafting resulted from a SPAAC reaction since omitting BCN (DOC: 0) or azide (008-F, RAN Biotechologies) completely abrogated antibody relocation to droplet inner surface and the fluorescence remained homogenously distributed in the droplets' lumen (**Figure S1**). Taken together, these results show that complete antibody grafting can be obtained with a DOC of 4 and 5 respectively with the tetra azide and the diazide fluorosurfactant. Consequently, we decided to pursue the study with an average DOC of 5.0 and tetra-azide fluorosurfactant (**3**) to limit the fraction of residual non-grafted antibody in the droplets. The size distribution of droplets was studied using a method previously published by Chowdhury *et al.*[25] and the droplet size distribution of the emulsion stabilized by the fluorosurfactant **3** showed a coefficient of variation of 5.1% after 2 h (**Figure S2**).

Immunosandwich display at the droplet surface

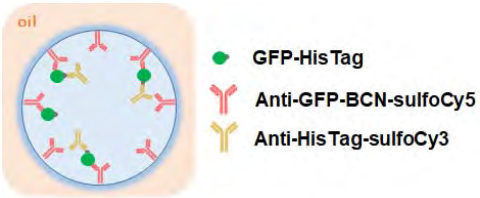

Figure 5. Schematic illustration of the immune sandwich at the inner droplet surface for the detection of GFP as model analyte. Format of immunosandwich: AntiGFP/GFP-HisTag/AntiHisTag. The sulfoCy5 labeled anti-GFP Ab is grafted at the inner surface of the droplet *via* SPAAC with the tetraazide surfactant. The GFP-HisTag is captured by the grafted antibody and thus relocates at the inner surface of the droplet. The sulfoCy3-labeled anti-HisTag Ab used as the detection antibody bind to the Ab/GFP complex via recognition of GFP's HisTag, and consequently also relocates at the inner surface.

We next extended the concept to other antibodies and sought to use them in order to capture a target protein, or ultimately form immunosandwiches at the droplet inner surface. To be able to easily track the localization of the antigen, we chose a His-tagged version of the Green Fluorescent Protein (GFP-HisTag) as a model target protein. Besides, we selected a pair of antibodies targeting two different epitopes (the GFP itself and the His-tag appended to the protein), one of which would be grafted at the inner surface of droplets and the other serving as detection antibody (**Figure 5**). Therefore, upon sandwich formation, not only the antigen but also the detection antibody should relocate at the surface. On the contrary, in the absence of the target protein, the second antibody should remain homogeneously distributed in the droplets.

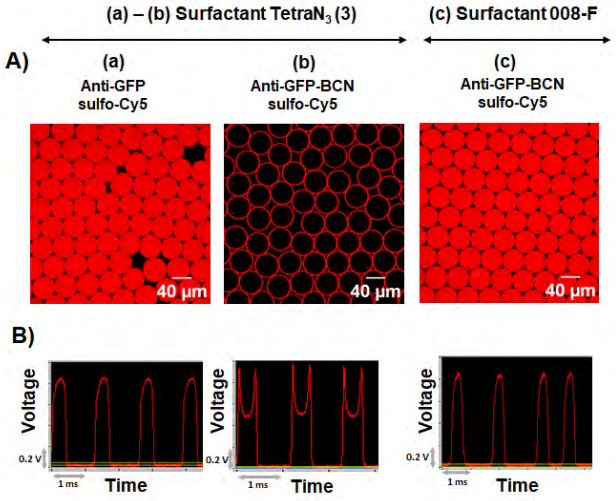

Figure 6. A) Confocal imaging and **B)** PMT signals of the encapsulation step between functionalized antibodies and the tetraazide fluorosurfactant **3** or the non-functionalized surfactant 008-F as a negative control. Conditions for droplets production: oil phase – Surfactant **3** ((a), (b)) or 008-F (c) (2.5% in Novec 7500); aqueous phase – CHAPS (1 mM in PBS 1X) (a) Anti-GFP-sulfoCy5 (400 nM), (b) Anti-GFP-BCN-sulfoCy5 (400 nM), (c) Anti-GFP-BCN-sulfoCy5 (400 nM).

To be able to monitor all the components of the system, both antibodies (the anti-HisTag and anti-GFP antibody) were also conjugated with distinct fluorescent dyes (sulfoCy3 and sulfoCy5, respectively). Two sets of antibodies (AntiGFP-sulfoCy5-BCN/AntiHisTag-sulfoCy3 and AntiHisTag-sulfoCy3-BCN/AntiGFP-sulfoCy5) were then prepared in which only one fluorescently labelled antibody bore a BCN moiety (DOC of 5). To assess the proper reactivity of these molecules with the droplet inner surface, each set of antibodies (final concentration of 400 nM) was encapsulated into 45 pL droplets stabilized with the surfactant **3**, or the surfactant 008-F as a negative control (**Figure 6 and Figure S3**). As expected, confocal imaging confirmed that SPAAC reaction had only occurred between azide-containing fluorosurfactants and BCN-functionalized antibodies (i.e. anti-GFP-BCN-sulfoCy5 and anti-HisTag-BCN-sulfoCy3 (**Figure 6 (b), Figure S3 and S4)**. This was also confirmed by online fluorescence profiling of droplets reinjected into a microfluidic device and showing a characteristic U-shaped signal, indicating fluorescence relocation at the inner surface of the droplet. In negative controls, when one of two bioorthogonal reaction partners is missing, either the azide or the BCN, a homogenous repartition of the fluorescence within droplets is observed, with online fluorescence profiling showing the typical "bell shape" signal of droplets containing a homogeneous diffuse fluorescence.

Having established the proper behaviour and specificity of antibodies, their ability to bind their target and form an immunosandwich grafted at the droplet surface was next tested. An aqueous phase made of 400 nM Anti-GFP-BCN-sulfoCy5, 125 nM GFP-HisTag and 50 nM anti-HisTag-sulfoCy3 was dispersed into 45 pL sized droplets stabilized by 2.5% surfactant **3**. Both confocal microscopy and online fluorescence profiling showed the co-localization of the three components of the sandwich at the inner surface of the droplets (**Figure 7**). Interestingly, we

found that the sandwich could be readily reversed (i.e., anti-HisTag antibody grafted at the droplet inner surface and anti-GFP antibody used for detection), with minimal impact on fluorescence relocation (**Figure S5**), highlighting the robustness of our technology. Moreover, replacing one of the specific antibodies by non-relevant Trastuzumab, did not lead to any capture of GFP and/or immunosandwich formation (**Figure S6** and **S7**). Taken together, these results not only indicate that the grafting of the antibody does not impair its ability to bind its target, but also that this first binding of the antigen does not prevent the recognition of the second epitope. Moreover, the absence of marked coalescence indicated that, even though a large molecular complex is formed, the surfactant **3** preserved its capacity to stabilize droplets.

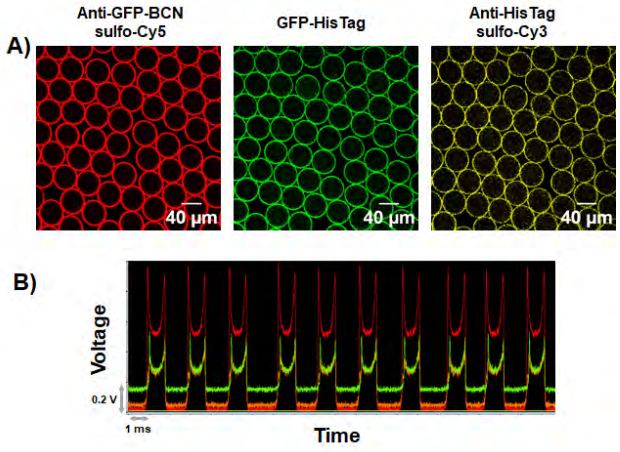

Figure 7. A) Confocal imaging and **B)** PMT signals of for both immune sandwiches format. Conditions for droplets production: oil phase – Surfactant **3** (2.5% in Novec 7500); aqueous phase – CHAPS (1 mM in PBS 1X); Anti-GFP-BCN-sulfoCy5 (400 nM), GFP-HisTag (125 nM), Anti-HisTag-sulfoCy3 (50 nM).

Protein detection

To evaluate the ability to detect proteins using D-SIRe, the concentration of GFP-HisTag in the droplets was varied from 25 to 150 nM, while the concentrations of the two sandwich antibodies were kept constant, anti-HisTag-BCN-sulfoCy3 at 400 nM, and anti-GFP-sulfoCy5 at 50 nM. It is noteworthy that since the droplets have a volume of 45 pL and the concentration of the detection antibody was kept constant at 50 nM, the amount of detection antibody is about 2.25 attomoles per droplet.

The intensity of the green "U shape" signal accounting for the concentration in GFP gradually decreased when the GFP concentration decreased (**Figure 8**). Interestingly it was still clearly visible even at the lowest concentration. The intensity of the detection antibody (red) remained comparable since the concentration of this antibody was maintained constant. However, the shape of the detection antibody signal (red) gradually evolved from "bell shape" to "U shape" when the amount of GFP increased. It thus appears that the limit of detection, defined as the inflexion point at which the change in signal shape can be detected, is lower than 50 nM / 2.3 attomoles of GFP per droplet. These results suggest that under the conditions used in our experiments, the D-SIRe is sensitive to low attomole amount of analyte and that signal shape report for analyte concentration. The range in which the relocation index increases as a function of analyte concentration was further evaluated. The amount of GFP was varied from 25 to 150 nM keeping the concentration of detection Ab constant at 50 nM. As anticipated the best dynamic range of response was observed around the concentration of the detection Ab, from 50 to 100 nM with an increase of R.I. from 4 to 17. When increasing further the concentration of analyte the R.I. reached a plateau. (**Figure S8**).

Immunosandwich assembly at droplet surface

In the previous experiments, since the different components were premixed prior to being emulsified, it is difficult to know if the sandwich had assembled at the surface of the droplets or if it had already formed prior to being grafted as a whole at the surface. To validate that the sandwich can assemble on an already grafted capture antibody, we prepared an emulsion in which the set of antibodies was encapsulated in the absence of GFP-HisTag. Then, upon a thirty minutes incubation, the target protein was picoinjected into the droplets and the fluorescence of the resulting emulsion was analyzed (**Figure S9**). This experiment confirmed that the sandwich still forms with an already immobilized antibody, provided GFP-HisTag was injected into the droplet (compare orange and blue circled cases on **Figure S9**).

Immunoassay of protein released from cells lysed in situ

To evaluate the capacity of D-SIRe to work in complex conditions, we challenged it to detect a specific cytoplasmic protein produced by a single cell. For this purpose, an *E. coli* strain producing the GFP-HisTag was encapsulated with the set of antibodies used above (Anti-GFP-sulfoCy5-BCN and Anti-HisTag-sulfoCy3). To make the cytoplasmic content accessible while avoiding premature cell lysis before encapsulation, the cell suspension was co-flown 1:1 on-chip with a lysis solution (400 nM anti-GFP-BCN-sulfoCy5, 50 nM anti-HisTag-sulfoCy3 and 10 mg/mL lysosyme in PBS 1X)) to form 45 pL droplets stabilized by surfactant **3** (2.5% in oil phase). Upon droplet formation, both aqueous solution mixed, triggering *E. coli* lysis and the release of the cytoplasmic content within the droplets. The average copies of *E.coli* per droplet were 0.8-0.9, and the distribution of *E.coli* in the droplets followed the Poisson law, with ~45% of droplets empty,~35% containing a single *E.coli*, ~15% encapsulating two *E.coli* and less than ~5% with more than two *E.coli* (See **Suporting Informations 3.2 for details**).[26,27]

Both confocal imaging and online fluorescence profiling confirmed that the grafting of Anti-GFP-BCN-sulfoCy5 antibody had taken place (**Figure 9**). Several droplets were left unoccupied by *E.coli*. They were therefore deprived of GFP (so did not display green fluorescence) and displayed a homogenously distributed yellow fluorescence (anti-HisTag-sulfoCy3) accounting for the absence of immunosandwich (**Figure 9, blue circled event**). This was confirmed by the "bell shape" signal recorded during the online fluorescence profiling. The remaining droplets were occupied by a bacterium and therefore displayed a green fluorescence. Since lysozyme does not produce an immediate lysis, different stages were readily distinguishable. First, the majority (~ 50 %) of the bacteria were completely lysed (no green cell visible in the droplet) and the released GFP-HisTag was entirely captured at the inner surface of the droplets (**Figure 9, yellow circled case**). Moreover, as expected, the immunosandwich formed and the anti-HisTag antibody relocated at the surface of the droplet as well. Here again, confocal imaging was confirmed by online fluorescence profiling showing the typical "U shape" signal for the three signals components. In a

second set of droplets, green intense spots were observed without any immunosandwich detected at the droplet's inner surface

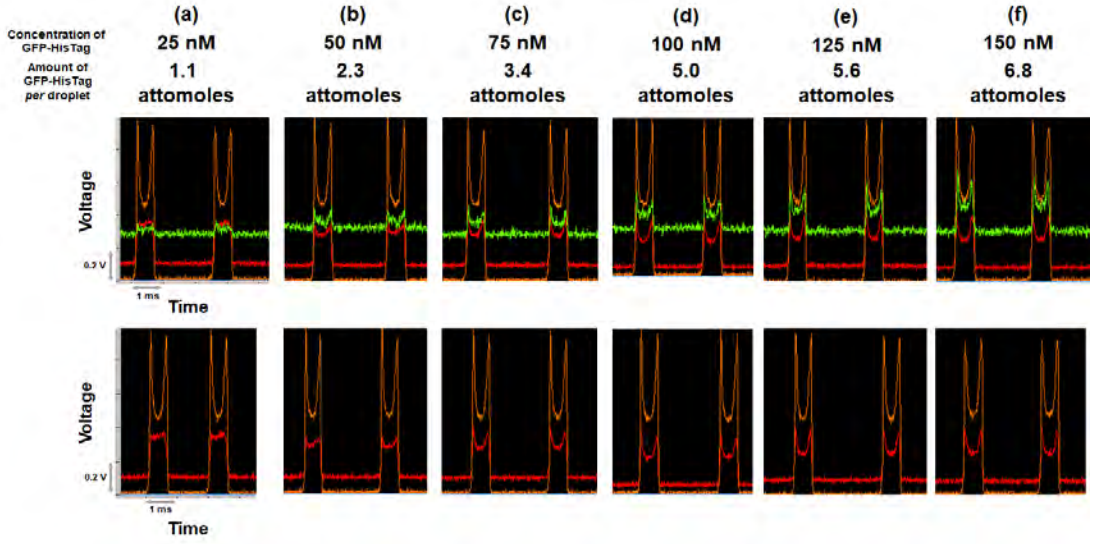

Figure 8. PMT signals of the Droplet Surface ImmunoAssay with increasing amount of GFP-HisTag. Conditions for droplets production: oil phase – Surfactant **3** (2.5% in Novec 7500); aqueous phase – CHAPS (1 mM in PBS 1X), Anti-GFP-BCN-sulfoCy5 (400 nM), GFP-HisTag, Anti-HisTag-sulfoCy3 (50 nM); Concentration of GFP-HisTag: (a) 25 nM; (b) 50 nM; (c) 75 nM; (d) 100 nM; (e) 125 nM; (f) 150 nM. **A)** PMT signals with laser at 488, 532 and 642 nm **B)** Signals obtained with the 488 nm laser signal removed.

(**Figure 9, magenta circled case**). These clusters likely correspond to non-lysed bacteria that did not release GFP. Finally, in few cases, an intermediate situation was observed with the presence of both a fluorescent particle and an immunosandwich (**Figure 9, green circled case**). This last case likely corresponds to partially lysed bacteria that released only a fraction of their content. Altogether these results confirm that the immunosandwich can assemble at the surface of the droplets using a protein released in a complex cellular environment as target antigen and that its sensitivity is compatible with the individual analysis of cells as small as bacteria.

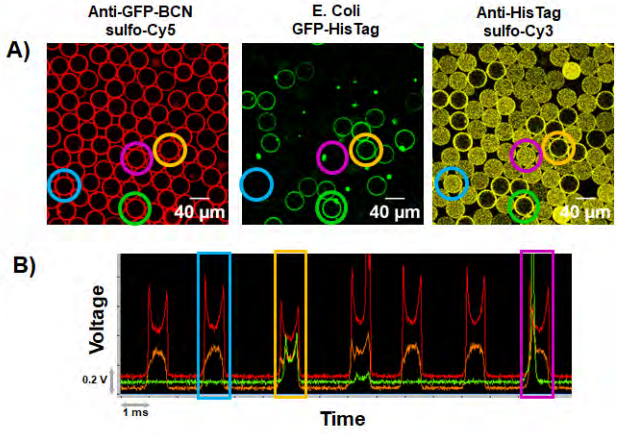

Figure 9. A) Confocal imaging and **B)** PMT signals of the encapsulation of *E. coli* in lysis buffer. Conditions for droplets production: oil phase – Surfactant **3** (2.5% in Novec 7500); aqueous phase 1 – CHAPS (1 mM in PBS 1X), Lysosyme (10 mg/mL in PBS 1X), Anti-GFP-BCN-sulfoCy5 (400 nM), Anti-HisTag-sulfoCy3 (50 nM); aqueous phase 2 – CHAPS (1 mM in PBS 1X), E.Coli (Transformed by plasmide to produce GFP-HisTag). Droplet content: 1:1 aq. phase 1/aq. phase 2. Circled in blue: droplet whithout *E. coli*, Circled in pink: droplet encapsulating non-lysed *E. coli*, circled in yellow: droplet encapsulating a lysed *E. coli*.

Conclusion

The work describes the synthesis of functionalized azide-PEG-PFPE-based fluorosurfactants and their reaction *via* SPAAC with strained alkyne conjugated antibodies at the inner water-oil interface of microfluidic droplets. The covalent bond formation process is not affected by lysis buffer or complex cell content. The resulting antibody-grafted surfactant maintains its ability to stabilize droplets and the capacity of the linked antibody to bind other proteins. This opened the possibility to form functional immunosandwich at the inner droplet surface. The characteristic shape of the fluorescence signal of the labeled detection antibody allows to measure its bound/unbound ratio without need of washing step. This new mode of detection in droplet microfluidic proved to be sensitive enough to allow detection of cytosolic proteins from a single lysed bacteria. The reported results and the novel fluorescence relocation read-out open interesting prospects in the field of single-cell droplet microfluidic, for cytosolic protein analysis, but also for secreted proteins analysis at the single cell level.

Materials and Methods

Microfluidic experimental setup:

Droplets production (two entries chip): Droplets were produced in two-entries chips. Flow rates were controlled by Fluigent software. Flow rates of 1000 µL/h for aqueous phase and of 1200-1400 µL/h for fluorinated oil phase (3M HFE 7500) were used to create droplets of 40-50 pL. Emulsion was collected in an Eppendorf filled with oil and closed with a PDMS plug to prevent coalescence due to contact with air. For control experiments, 2.5% w/w of non-functionalized surfactant (008-FluoroSurfactant, RAN Biotechnologies) was used in oil phase. For SPAAC reaction, the functionalized surfactant were used at 2.5% w/w in oil phase. Biomolecules were

introduced *via* the aqueous phase and dissolved in CHAPS (1 mM in PBS 1X).

Droplets production for cell encapsulation (three entries chip): Droplets were produced in three-entries chips. Flow rates were controlled by Fluigent software. Flow rates of 500 µL/h for aqueous phase 1 and 2 and of 1000-1200 µL/h for fluorinated oil phase (3M HFE 7500) were used to create droplets of 40-50 pL. Emulsion was collected in an Eppendorf filled with oil and closed with a PDMS plug to prevent coalescence due to contact with air. For SPAAC reaction, the functionalized surfactant were used at 2.5% w/w in oil phase. Biomolecules were introduced *via* one aqueous phase and dissolved in CHAPS (1 mM in PBS 1X). E.Coli were brought *via* the second aqueous phase in PBS 1X. Aqueous phases had identical flow rates in order for the ratio of the two aqueous phases in the droplet to be 1:1.

Picoinjection: Picoinjection were done in three entries chips. Flow rates were controlled by Fluigent software. Flow rates of 1700 µL/h for fluorinated oil phase (3M HFE 7500), 1000 µL/h for emulsion sample, and 180 µL/h for picoinjected solution were used to picoinject droplets. Droplets were destabilized by continuous electric impulses with a frequence of 30 kHz and an amplitude of 400 mV. Emulsion was collected in an Eppendorf filled with oil and closed with a PDMS plug to prevent coalescence due to contact with air. The functionalized surfactant were used at 2.5% w/w in oil phase. Biomolecules were picoinjected *via* the aqueous phase and dissolved in CHAPS (1 mM in PBS 1X).

Reinjection: W/O emulsions were reinjected in the second chip and spaced by fluorous oil (3M HFE 7500). Flow rates of 300 µL/h for HFE 7500 and of 100 µL/h for emulsion sample were used.

ASSOCIATED CONTENT

Supporting Information

The Supporting Information is available free of charge on the ACS Publications website.

Additional experimental details such as materials, methods, synthesis route and protocols, molecules characterization (NMR, FT-IR, HRMS), bioconjugaison procedures, microfluidic experiments setup and procedures, additional figures with confocal microscopy imaging and PMT signal. (PDF)

AUTHOR INFORMATION

Corresponding Author

*Alain Wagner, [1]Bio-Functional Chemistry (UMR 7199), LabEx Medalis, ICFRC, University of Strasbourg, 74 Route du Rhin, 67400 Illkirch-Graffenstaden, France,
Email: alwag@unistra.fr
https://orcid.org/0000-0003-3125-601X

Author Contributions

The manuscript was written through contributions of all authors. All authors have given approval to the final version of the manuscript.

ACKNOWLEDGMENT

Performed within Interdisciplinary Thematic Institute "IMCBio" (ITI 2021-2028 program of University of Strasbourg, CNRS and Inserm), this work was also supported by IdEx Unistra (ANR-10-IDEX-0002), SFRI-STRAT'US project (ANR-20-SFRI0012), EUR IMCBio (ANR-17-EURE-0023) under the framework of the French Investments for the Future Program, the previous LabEx NetRNA (ANR-10-LABX-0036), and also supported by Centre National de la Recherche Scientifique (CNRS), Université de Strasbourg, and its Initiative of Excellence (IdEx).

REFERENCES

(1) Uhlén, M.; Karlsson, M. J.; Hober, A.; Svensson, A.-S.; Scheffel, J.; Kotol, D.; Zhong, W.; Tebani, A.; Strandberg, L.; Edfors, F.; Sjöstedt, E.; Mulder, J.; Mardinoglu, A.; Berling, A.; Ekblad, S.; Dannemeyer, M.; Kanje, S.; Rockberg, J.; Lundqvist, M.; Malm, M.; Volk, A.-L.; Nilsson, P.; Månberg, A.; Dodig-Crnkovic, T.; Pin, E.; Zwahlen, M.; Oksvold, P.; von Feilitzen, K.; Häussler, R. S.; Hong, M.-G.; Lindskog, C.; Ponten, F.; Katona, B.; Vuu, J.; Lindström, E.; Nielsen, J.; Robinson, J.; Ayoglu, B.; Mahdessian, D.; Sullivan, D.; Thul, P.; Danielsson, F.; Stadler, C.; Lundberg, E.; Bergström, G.; Gummesson, A.; Voldborg, B. G.; Tegel, H.; Hober, S.; Forsström, B.; Schwenk, J. M.; Fagerberg, L.; Sivertsson, Å. The Human Secretome. *Sci. Signal.* **2019**, *12* (609), eaaz0274. https://doi.org/10.1126/scisignal.aaz0274.

(2) Geyer, P. E.; Kulak, N. A.; Pichler, G.; Holdt, L. M.; Teupser, D.; Mann, M. Plasma Proteome Profiling to Assess Human Health and Disease. *Cell Syst.* **2016**, *2* (3), 185–195. https://doi.org/10.1016/j.cels.2016.02.015.

(3) Ellington, A. A.; Kullo, I. J.; Bailey, K. R.; Klee, G. G. Antibody-Based Protein Multiplex Platforms: Technical and Operational Challenges. *Clin. Chem.* **2010**, *56* (2), 186–193. https://doi.org/10.1373/clinchem.2009.127514.

(4) Bendes, A.; Dale, M.; Mattsson, C.; Dodig-Crnković, T.; Iglesias, M. J.; Schwenk, J. M.; Fredolini, C. Bead-Based Assays for Validating Proteomic Profiles in Body Fluids. *Protein Microarrays for Disease Analysis: Methods and Protocols*, 2021, 65–78. https://doi.org/10.1007/978-1-0716-1562-1_5.

(5) Shah, K.; Maghsoudlou, P. Enzyme-Linked Immunosorbent Assay (ELISA): The Basics. *Br. J. Hosp. Med.* **2016**, *77* (7), C98–C101. https://doi.org/10.12968/hmed.2016.77.7.C98.

(6) Hosseini, S.; Vázquez-Villegas, P.; Rito-Palomares, M.; Martinez-Chapa, S. O. Advantages, Disadvantages and Modifications of Conventional ELISA. *Enzyme-linked Immunosorbent Assay (ELISA): From A to Z*, 2018, 67–115. https://doi.org/10.1007/978-981-10-6766-2_5.

(7) Hosseini, S.; Ibrahim, F.; Djordjevic, I.; Rothan, H. A.; Yusof, R.; van der Marel, C.; Benzina, A.; Koole, L. H. Synthesis and Characterization of Methacrylic Microspheres for Biomolecular Recognition: Ultrasensitive Biosensor for Dengue Virus Detection. *Eur. Polym. J.* **2014**, *60*, 14–21. https://doi.org/10.1016/j.eurpolymj.2014.08.010.

(8) Tekin, H. C.; Gijs, M. A. M. Ultrasensitive Protein Detection: A Case for Microfluidic Magnetic Bead-Based Assays. *Lab. Chip* **2013**, *13* (24), 4711–4739. https://doi.org/10.1039/C3LC50477H.

(9) Bowman, E. K.; Alper, H. S. Microdroplet-Assisted Screening of Biomolecule Production for Metabolic Engineering Applications. *Trends Biotechnol.* **2020**, *38* (7), 701–714. https://doi.org/10.1016/j.tibtech.2019.11.002.

(10) Cohen, L.; Cui, N.; Cai, Y.; Garden, P. M.; Li, X.; Weitz, D. A.; Walt, D. R. Single Molecule Protein Detection with Attomolar Sensitivity Using Droplet Digital Enzyme-Linked Immunosorbent Assay. *ACS Nano* **2020**, *14* (8), 9491–9501. https://doi.org/10.1021/acsnano.0c02378.

(11) Ding, R.; Hung, K.-C.; Mitra, A.; Ung, L. W.; Lightwood, D.; Tu, R.; Starkie, D.; Cai, L.; Mazutis, L.; Chong, S.; Weitz, D. A.; Heyman, J. A. Rapid Isolation of Antigen-Specific B-Cells Using Droplet Microfluidics. *RSC Adv.* **2020**, *10* (45), 27006–27013. https://doi.org/10.1039/D0RA04328A.

(12) Gérard, A.; Woolfe, A.; Mottet, G.; Reichen, M.; Castrillon, C.; Menrath, V.; Ellouze, S.; Poitou, A.; Doineau, R.; Briseno-Roa, L.; Canales-Herrerias, P.; Mary, P.; Rose, G.; Ortega, C.; Delincé, M.; Essono, S.; Jia, B.; Iannascoli, B.; Richard-Le Goff, O.; Kumar, R.; Stewart, S. N.; Pousse, Y.; Shen, B.; Grosselin, K.; Saudemont, B.; Sautel-Caillé, A.; Godina, A.; McNamara, S.; Eyer, K.; Millot, G. A.; Baudry, J.; England, P.; Nizak, C.; Jensen, A.; Griffiths, A. D.; Bruhns,

P.; Brenan, C. High-Throughput Single-Cell Activity-Based Screening and Sequencing of Antibodies Using Droplet Microfluidics. *Nat. Biotechnol.* **2020**, *38* (6), 715–721. https://doi.org/10.1038/s41587-020-0466-7.

(13) Eyer, K.; Doineau, R. C. L.; Castrillon, C. E.; Briseño-Roa, L.; Menrath, V.; Mottet, G.; England, P.; Godina, A.; Brient-Litzler, E.; Nizak, C.; Jensen, A.; Griffiths, A. D.; Bibette, J.; Bruhns, P.; Baudry, J. Single-Cell Deep Phenotyping of IgG-Secreting Cells for High-Resolution Immune Monitoring. *Nat. Biotechnol.* **2017**, *35* (10), 977–982. https://doi.org/10.1038/nbt.3964.

(14) Matuła, K.; Rivello, F.; Huck, W. T. S. Single-Cell Analysis Using Droplet Microfluidics. *Adv. Biosyst.* **2020**, *4* (1), 1900188. https://doi.org/10.1002/adbi.201900188.

(15) Khater, A.; Mohammadi, M.; Mohamad, A.; Nezhad, A. S. Dynamics of Temperature-Actuated Droplets within Microfluidics. *Sci. Rep.* **2019**, *9* (1), 3832. https://doi.org/10.1038/s41598-019-40069-9.

(16) Etienne, G.; Kessler, M.; Amstad, E. Influence of Fluorinated Surfactant Composition on the Stability of Emulsion Drops. *Macromol. Chem. Phys.* **2017**, *218* (2), 1600365. https://doi.org/10.1002/macp.201600365.

(17) Holtze, C.; Rowat, A. C.; Agresti, J. J.; Hutchison, J. B.; Angilè, F. E.; Schmitz, C. H. J.; Köster, S.; Duan, H.; Humphry, K. J.; Scanga, R. A.; Johnson, J. S.; Pisignano, D.; Weitz, D. A. Biocompatible Surfactants for Water-in-Fluorocarbon Emulsions. *Lab. Chip* **2008**, *8* (10), 1632–1639. https://doi.org/10.1039/b806706f.

(18) Kreutz, J. E.; Li, L.; Roach, L. S.; Hatakeyama, T.; Ismagilov, R. F. Laterally Mobile, Functionalized Self-Assembled Monolayers at the Fluorous–Aqueous Interface in a Plug-Based Microfluidic System: Characterization and Testing with Membrane Protein Crystallization. *J. Am. Chem. Soc.* **2009**, *131* (17), 6042–6043. https://doi.org/10.1021/ja808697e.

(19) Ursuegui, S.; Mosser, M.; Wagner, A. Copper-Free Click Chemistry for Microdroplet's W/O Interface Engineering. *RSC Adv.* **2016**, *6* (97), 94942–94948. https://doi.org/10.1039/C6RA20385J.

(20) Chowdhury, M. S.; Zhang, X.; Amini, L.; Dey, P.; Singh, A. K.; Faghani, A.; Schmueck-Henneresse, M.; Haag, R. Functional Surfactants for Molecular Fishing, Capsule Creation, and Single-Cell Gene Expression. *Nano-Micro Lett.* **2021**, *13* (1), 147. https://doi.org/10.1007/s40820-021-00663-x.

(21) Ursuegui, S.; Schneider, J. P.; Imbs, C.; Lauvoisard, F.; Dudek, M.; Mosser, M.; Wagner, A. Expedient Synthesis of Trifunctional Oligoethyleneglycol-Amine Linkers and Their Use in the Preparation of PEG-Based Branched Platforms. *Org. Biomol. Chem.* **2018**, *16* (44), 8579–8584. https://doi.org/10.1039/C8OB02097C.

(22) Chowdhury, M. S.; Zheng, W.; Kumari, S.; Heyman, J.; Zhang, X.; Dey, P.; Weitz, D. A.; Haag, R. Dendronized Fluorosurfactant for Highly Stable Water-in-Fluorinated Oil Emulsions with Minimal Inter-Droplet Transfer of Small Molecules. *Nat. Commun.* **2019**, *10* (1), 4546. https://doi.org/10.1038/s41467-019-12462-5.

(23) Gruner, P.; Riechers, B.; Semin, B.; Lim, J.; Johnston, A.; Short, K.; Baret, J.-C. Controlling Molecular Transport in Minimal Emulsions. *Nat. Commun.* **2016**, *7* (1), 10392. https://doi.org/10.1038/ncomms10392.

(24) Roach, L. S.; Song, H.; Ismagilov, R. F. Controlling Nonspecific Protein Adsorption in a Plug-Based Microfluidic System by Controlling Interfacial Chemistry Using Fluorous-Phase Surfactants. *Anal. Chem.* **2005**, *77* (3), 785–796. https://doi.org/10.1021/ac049061w.

(25) Chowdhury, M. S.; Zheng, W.; Singh, A. K.; Ong, I. L. H.; Hou, Y.; Heyman, J. A.; Faghani, A.; Amstad, E.; Weitz, D. A.; Haag, R. Linear Triglycerol-Based Fluorosurfactants Show High Potential for Droplet-Microfluidics-Based Biochemical Assays. *Soft Matter* **2021**, *17* (31), 7260–7267. https://doi.org/10.1039/D1SM00890K.

(26) Mazutis, L.; Gilbert, J.; Ung, W. L.; Weitz, D. A.; Griffiths, A. D.; Heyman, J. A. Single-Cell Analysis and Sorting Using Droplet-Based Microfluidics. *Nat. Protoc.* **2013**, *8* (5), 870–891. https://doi.org/10.1038/nprot.2013.046.

(27) Geersens, É.; Vuilleumier, S.; Ryckelynck, M. Growth-Associated Droplet Shrinkage for Bacterial Quantification, Growth Monitoring, and Separation by Ultrahigh-Throughput Microfluidics. *ACS Omega* **2022**, *7* (14), 12039–12047. https://doi.org/10.1021/acsomega.2c00248.

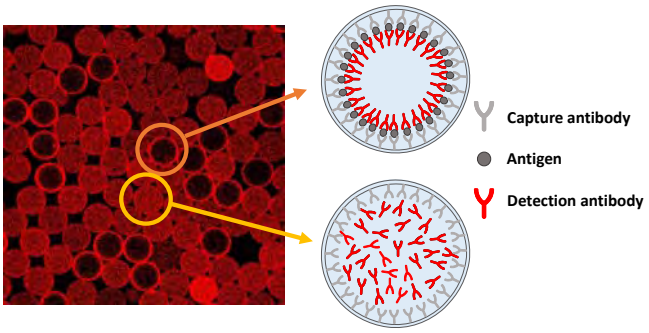

For Table of Content only